ORIGINAL ARTICLE

The predictive value of pretherapy [^{68}Ga]Ga-DOTA-TATE PET and biomarkers in [^{177}Lu]Lu-PRRT tumor dosimetry

Azadeh Akhavanallaf[1,2] · Avery B. Peterson[1] · Kellen Fitzpatrick[1] · Molly Roseland[1] · Ka Kit Wong[1] · Issam El-Naqa[3] · Habib Zaidi[2,4,5,6] · Yuni K. Dewaraja[1]

Abstract

Purpose Metastatic neuroendocrine tumors (NETs) overexpressing type 2 somatostatin receptors are the target for peptide receptor radionuclide therapy (PRRT) through the theragnostic pair of ^{68}Ga/^{177}Lu-DOTATATE. The main purpose of this study was to develop machine learning models to predict therapeutic tumor dose using pre therapy ^{68}Ga -PET and clinicopathological biomarkers.
Methods We retrospectively analyzed 90 segmented metastaticNETs from 25 patients (M14/F11, age 63.7 ± 9.5, range 38–76) treated by ^{177}Lu-DOTATATE at our institute. Patients underwent both pretherapy [^{68}Ga]Ga-DOTA-TATE PET/CT and four timepoints SPECT/CT at ~ 4, 24, 96, and 168 h post-^{177}Lu-DOTATATE infusion. Tumors were segmented by a radiologist on baseline CT or MRI and transferred to co-registered PET/CT and SPECT/CT, and normal organs were segmented by deep learning-based method on CT of the PET and SPECT. The SUV metrics and tumor-to-normal tissue SUV ratios (SUV_TNRs) were calculated from ^{68}Ga -PET at the contour-level. Posttherapy dosimetry was performed based on the co-registration of SPECT/CTs to generate time-integrated-activity, followed by an in-house Monte Carlo-based absorbed dose estimation. The correlation between delivered ^{177}Lu Tumor absorbed dose and PET-derived metrics along with baseline clinicopathological biomarkers (such as Creatinine, Chromogranin A and prior therapies) were evaluated. Multiple interpretable machine-learning algorithms were developed to predict tumor dose using these pretherapy information. Model performance on a nested tenfold cross-validation was evaluated in terms of coefficient of determination (R^2), mean-absolute-error (MAE), and mean-relative-absolute-error (MRAE).
Results SUV$_{mean}$ showed a significant correlation (q-value < 0.05) with absorbed dose (Spearman $\rho = 0.64$), followed by TLSUV$_{mean}$ (SUV$_{mean}$ of total-lesion-burden) and SUV$_{peak}$ ($\rho = 0.45$ and 0.41, respectively). The predictive value of PET-SUV$_{mean}$ in estimation of posttherapy absorbed dose was stronger compared to PET-SUV$_{peak}$, and SUV_TNRs in terms of univariate analysis ($R^2 = 0.28$ vs. $R^2 \leq 0.12$). An optimal trivariate random forest model composed of SUV$_{mean}$, TLSUV$_{mean}$, and total liver SUV$_{mean}$ (normal and tumoral liver) provided the best performance in tumor dose prediction with $R^2 = 0.64$, MAE = 0.73 Gy/GBq, and MRAE = 0.2.
Conclusion Our preliminary results demonstrate the feasibility of using baseline PET images for prediction of absorbed dose prior to ^{177}Lu-PRRT. Machine learning models combining multiple PET-based metrics performed better than using a single SUV value and using other investigated clinicopathological biomarkers. Developing such quantitative models forms the groundwork for the role of ^{68}Ga -PET not only for the implementation of personalized treatment planning but also for patient stratification in the era of precision medicine.

Keywords Dosimetry · Theragnostic · 177Lu-DOTATATE · Machine learning

Introduction

The theragnostic principle has been summed up as: "We treat what we see, and We see what we treat"[1] [1]. This concept of "see and treat" in nuclear medicine therapy has led to

___
[1] Prof. Richard Baum.

This article is part of the Topical Collection on Theragnostic.

✉ Azadeh Akhavanallaf
azadehak@med.umich.edu

Extended author information available on the last page of the article

the development of theragnostic pairs, consisting of an imaging radiotracer for staging and molecular targeting and its therapeutic counterpart, usually a *beta-* or *alpha*-emitter for tumor ablation. Neuroendocrine tumors (NETs) commonly express somatostatin receptors (SSTR), predominantly subtype 2, which is the basis for the use of SSTR PET imaging and peptide receptor radionuclide therapy (PRRT). For the management of NET, the theragnostic pair of ^{68}Ga/^{177}Lu-DOTA-TATE has been widely used since 2018 when [^{177}Lu]Lu-DOTA-TATE (Lutathera) was approved by the US Food and Drug Administration (FDA) on the basis of NETTER-1 trial results [2, 3].

In current ^{177}Lu-PRRT clinical practice, pretherapy [^{68}Ga]Ga-DOTATATE (^{68}Ga-PET) is required for candidate eligibility to confirm sufficient tumor SSTR expression (peformed via qualitative assessment with Krenning score). The approved empiric protocol for ^{177}Lu-PRRT is 4 cycles of 7.4 GBq infusions (∼2 months intervals). Although ^{177}Lu-PRRT has been showed to improve progression-free survival (65% at 20 months, compared to long-acting octreotide 11%), objective responses are uncommon (20%) and complete responses are rare (1–2%). Therefore, to optimize ^{177}Lu-PRRT outcomes, either patient selection criteria must be improved or a personalized treatment approach must be developed. Precision nuclear medicine for PRRT has been proposed, with pretreatment ^{68}Ga-PET used for patient selection and additional posttherapy imaging valuable to provide individualized measurements relevant to treatment safety and efficacy [4].

Dosimetry-guided personalized ^{177}Lu-PRRT generally involves modulation of the number of treatment cycles or the administered dose per cycle based on pretherapy biomarkers or posttherapy imaging-based dosimetry, which has been shown to have a positive impact on treatment response [5, 6]. Predictions of therapy delivered absorbed doses from ^{177}Lu-PRRT have also been performed using pretherapy ^{68}Ga-PET, which is particularly desirable for planned alterations in the first cycle of ^{177}Lu-PRRT, which has the potential to maximize tumor absorbed dose while limiting toxicity to an acceptable level [7, 8]. Two previous studies [7, 9] reported on the ability to predict renal dose using pretherapy imaging, as the kidney toxicity is a limiting factor for ^{177}Lu-labeled RPTs [9]. Knowledge of expected renal dose exposure per cycle is especially important if escalation of administered activity is considered in the first RPT cycle; while not currently performed routinely in clinical practice, prioritizing higher doses early on may be preferable, since there is an observed decrease in absorbed tumor dose per administered activity (Gy/GBq) in subsequent cycles [10].

According to the principles of RPT and cellular irradiation, the likelihood of tumor response is expected to be correlated with the tumor absorbed dose. Various studies have shown dose-response correlations in ^{177}Lu-PRRT [3, 5, 11, 12]. Furthermore, some authors have reported on the correlation of ^{68}Ga-PET uptake with treatment outcome [13, 14]. In this context, tumor absorbed dose estimation prior to the therapy could provide a quantitative metric for response with potential to improve patient-selection criteria. However, the relationship between imaging agents of theragnostic pairs and therapy delivered dose is not straightforward. Previous studies reported on the correlation of pretherapy imaging PET metrics alone [15, 16] and combined with clinical biomarkers [7] with respect to posttherapy absorbed dose. The study by Xue et al. [7] used machine learning models in prediction of posttherapy absorbed dose for [^{177}Lu]Lu-PSMA

therapy. Compared to simple linear regression, data-driven machine learning algorithms by considering multivariate correlations of training data can minimize the uncertainties, thus improving the predictive power of the model.

We therefore sought to develop models that predict the mean tumor absorbed doses delivered by ^{177}Lu-DOTA-TATE using pretherapy [^{68}Ga]Ga-DOTA-TATE PET plus a comprehensive set of clinicopathological biomarkers. The contribution of this work to the field of RPT is threefold: (1) using a previously validated Monte Carlo-based dosimetry workflow with a patient cohort that includes four-posttherapy SPECT/CT scans [17], (2) including a complete set of clinical biomarkers in addition to ^{68}Ga-PET in the dosimetry prediction models, and (3) implementation of interpretable machine learning algorithms for dose prediction.

Materials and methods

Patient population

This study comprised of 25 patients with histologically proven metastatic NETs, progressive on prior therapy, who received at least the first cycle of standard ^{177}Lu-DOTA-TATE PRRT and underwent four timepoints SPECT/CT dosimetry at the University of Michigan Hospital. As part of an ongoing research study approved by the Institutional Review Board, all patients provided written informed consent to participate in the study, which included serial SPECT/CT imaging following standard treatment. Patients' demographic information is presented in supplemental-Table 1.

Tumor and organ delineation

Up to five index lesions larger than 2 mL were manually segmented by a radiologist (MER) on diagnostic-quality baseline CT or MRI. The criteria for inclusion of the lesions up to five for each patient were mainly based on the anatomical size and the clear margins in visualization in order to gain confidence in manual segmentation. Thereafter, the delineated index lesions were transferred to the subsequent PET/CT and SPECT/CT scans using co-registration. The spleen was manually segmented by a technologist while kidneys and liver were segmented using a deep learning algorithm on the CT of the PET/CT and SPECT/CT [17]. The normal liver was sampled from uniform uptake regions using three sphere volumes-of-interest (8 cm^3). The organ segmentations were verified and adjusted by the radiologist as needed.

[68]Ga PET/CT imaging and PET-derived metrics

Patient preparation required PET scans to be acquired 4 weeks after any long-acting somatostatin analogue treatment. PET/

CTs were acquired at ~60 min (range: 54–77 min) post-intravenous injection of ~160 MBq of [68Ga]Ga-DOTA-TATE (range: 144–196 MBq). Data were reconstructed using vendor-specific recommended parameters. A mean value partial volume correction was performed using volume dependent recovery coefficients (from a sphere-phantom measurement [2]) applied to SUVmean from pretherapy PET images.

Image-derived features, both activity and SUV (standardized uptake value) metrics, were calculated for the transferred contours. Tumor SUV metrics including mean, peak, coefficient of variation (CoV: standard deviation divided by SUV_{mean}), skewness and kurtosis, and mean activity (Bq/mL) corrected to the injection time and normalized by injected activity were extracted. In addition, SUV_{mean} of the spleen, healthy liver, and kidneys along with blood pool (SUV_{mean} in aortic arch) were quantified. The relative tumor uptake was calculated as tumor-to-normal tissue ratios (TNR) using tumor SUV_{mean} relative to the SUV_{mean} of normal spleen (SUV_TNR_{spleen}), normal liver (SUV_TNR_{liver}) and blood pool (SUV_TNR_{blood}). In addition, SUV_{mean} of the total liver volume encompassing both healthy tissue and lesions is quantified as $TotLiverSUV_{mean}$.

To quantify total lesion burden-related metrics, whole-body PET-SUV images were segmented using an empiric SUV threshold (whole-body SUV-cutoff = 5, liver SUV-cutoff = 10). The generated mask from thresholding was adjusted to add lesions not included in initial segmentation and removed physiological uptake in organs and then verified by the nuclear medicine clinician (KW). Therefore, three independent metrics based on the segmented mask encompassing total [68Ga]Ga-DOTA-TATE-avid lesion volume were defined: total lesion volume (TLV) in mL, average SUV of the total lesion volume ($TLSUV_{mean}$), and total lesion somatostatin expression (TL-SSE) defined as $TLV \times TLSUV_{mean}$.

Clinicopathological biomarkers

A total of 25 clinical, pathologic, and laboratory variables were included in our study, all of which we believed had theoretical potential to influence patient overall health, tumor behavior, and treatment response. Clinical patient data and lab values were obtained through review of the electronic medical record.

The total variable set, including 16 quantitative and 3 qualitative 68Ga-PET features, 8 treatment history, and 11 blood-test biomarkers, is detailed in Table 1.

177Lu SPECT/CT imaging and dosimetry workflow

Our patient data regarding dosimetry in patients undergoing [177Lu]Lu-DOTA-TATE comes from an ongoing research study that includes serial posttherapy SPECT/CT imaging at ~4, 24, 96, and 168 h after the first cycle. A 25 min single-bed SPECT/CT acquisition is performed on a Siemens Intevo using manufacturer-recommended protocol and reconstructed with Siemens xSPECT Quant using 48 iterations and 1 subset and no post filtering [18].

For dosimetry, we employed an integrated workflow implemented within MIM software that has been elaborated in a recent article by Dewaraja et al. [17]. The workflow is composed of the following steps:

1. A contour-guided intensity-based registration was used to align four posttherapy SPECT images.
2. Time integrated activity (TIA) was calculated by integration of the time-activity curve, a mono/bi-exponential function (TIA $= \int_{t_0}^{\infty} C(e^{-\lambda_1 t} - e^{-\lambda_2 t})$). Here, C scales the curve up or down, λ_1 is the clearance/elimination rate, and λ_2 is the uptake/absorption rate. The term effective half-life (T_{eff}) refers to the slower exponential component ($i.e. T_{eff} = \frac{\ln(2)}{\lambda_1} | \lambda_1 \ll \lambda_2$).
3. TIA along with the corresponding density map (obtained from CT) was coupled with a fast Monte Carlo (MC) simulator, developed at the University of Michigan [19], to generate the voxel-level absorbed dose map. Mean absorbed dose estimates for tumor and organ volumes included partial volume correction using volume dependent recovery coefficients (from a sphere-phantom measurement [2]).

Statistical analysis and predictive modeling

For the statistical analysis, the Spearman rank correlation between predictive features and tumor absorbed dose per unit administered activity were analyzed, followed by Benjamini and Hochberg p-value correction, where q-value < 0.05 considered significant.

To predict tumor absorbed dose using PET-derived features and biomarkers, a cross-combination of different supervised machine learning algorithms was analyzed where random forest outperformed other algorithms. Therefore, we presented the comparison between linear and supervised random forest regression algorithms through univariate, bivariate, and multivariate analysis implemented in MATLAB 2022 (MathWorks Inc., Natick, MA, USA). We adopted nested cross-validation (CV), whereby the outer-loop CV was repeated 10 times to consolidate the results of tenfold inner-loop CV [20]. During inner-loop CVs, 10% of the whole dataset was considered as unseen validation-set and 90% used as training-set. Due to the intrinsic heterogeneity and limited size of our data, bootstrap aggregation strategy (500 bootstrap samples with replacement) was implemented to improve model stability and avoid overfitting (algorithm flowchart in supplemental-Fig. 1).

Table 1 Complete variable set, including PET and clinicopathological features, used in the statistical analysis and the development of a predictive model for tumor delivered dose from ^{177}Lu-PRRT

Type of feature	Name of feature	Description
Shape	Volume	Volume of index tumors (segmented by radiologist)
PET uptake/SUV	SUV_{mean}	Mean SUV value
	SUV_{peak}	Average SUV within a 1 cm^3 sphere centered on the site of highest uptake in a tumor
	SUV_{kurt}	Measure of the shape of the peak of the SUV distribution (kurtosis)
	SUV_{skew}	Measure of the asymmetry of the SUV distribution (skewness)
	$SUV_{BloodPool}$	SUV_{mean} in the aortic arch
	SUV_{Spleen}	SUV_{mean} of the Spleen contour
	SUV_{Liver}	Average SUV_{mean} of three spheres (8 mL) sampled from the normal liver tissue
	$SUV_{Kidneys}$	Average of SUV_{mean} from right and left kidney contours
	SUV_TNR_{blood}	Ratio of Tumor SUV_{mean} to blood pool SUV_{mean}
	SUV_TNR_{spleen}	Ratio of Tumor SUV_{mean} to SUV_{mean} of the spleen
	SUV_TNR_{liver}	Ratio of Tumor SUV_{mean} to SUV_{mean} of the liver
	$TotLiverSUV_{mean}$	SUV_{mean} of the whole liver including both normal and tumoral tissues
	TLV	Total lesion volume
	$TL\text{-}SUV_{mean}$	Average SUV of the entire total lesion volume
	TL-SSE	Total lesion somatostatin expression (TLV × TL-SUV$_{mean}$)
Diagnostic	Liver metastasis	Disease present in liver (based on Dotatate PET)
	Bone metastasis	Disease present in bone (based on Dotatate PET)
	Node metastasis	Disease present in lymph nodes (based on Dotatate PET)
	Tumor location	Anatomical location of the index tumor
Histological	Grade	Histologic grade (using Ki67 index) of primary tumor from biopsy/surgery
	Primary tumor site	Primary tumor site
Treatments	#Systemic therapy	Number of prior systemic treatments (chemotherapy or other)
	#Directed therapy	Number of prior liver directed treatments (TACE, Y90, cryotherapy)
	Y90-SIRT	Prior treatment liver with Y90-SIRT
	Everolimus	Prior treatment with everolimus (systemic MTOR inhibitor)
	Capecitabine/temozolomide	Prior treatment with capecitabine and temozolomide (Chemo, systemic)
	Sunitinib	Prior treatment with Sunitinib (multi-kinase inhibitor, systemic)
Blood tests	White blood cells	White blood cells (K/cmm)
	Lymphocytes	Lymphocytes
	Absolute neutrophil	Absolute neutrophil counts (K/cmm)
	Hemoglobin	Hemoglobin (g/dL)
	Platelet	Platelet count (K/cmm)
	eGFR	Estimated glomerular filtration rate (calculated)
	Creatinine	Creatinine (mg/dL)
	Bilirubin	Bilirubin (mg/dL)
	Albumin	Albumin (mg/dL)
	Alkaline phosphatase	Alkaline phosphatase (ALK, ALP, ALKP, or ALK PHOS) (IU/L)
	CgA	Chromogranin A (tumor marker) (ng/mL)

We designed a hierarchical interpretable feature selection strategy using main-effect analysis to select the most important predictors. First, using a univariate linear regression model, the best variable with the highest coefficient of determination (R^2) was determined. In the second step, a set of bivariate regression models was generated using two independent variables, i.e., the selected variable from the univariate analysis followed by a second variable from the predictor-set. In the third step, the five best bivariate models that most increased predictive likelihood (with the highest R^2) were selected, forming the basis for a set of trivariate models. We extended the process up to four-variable models, but because we saw no further significant improvement in predictive likelihood, this process was stopped. In addition, we employed ElasticNet and Permutation-based Random Forest variable-Importance (PRFvI) feature selection

algorithms. The feature-selection algorithms were implemented in a bootstrap ensemble framework as elaborated in supplemental-Fig. 2. A maximum of 8 features were selected based on the recommended number of at least ten observations per predictor [21].

We employed the proposed hierarchical feature selection algorithm in both linear and random forest algorithms. In the linear model, we used a generalized linear regression model based on the least square loss function. In the case of random forest algorithms, we used a bootstrap aggregation between two models including random forest (ensemble tree) [22] and generalized additive model [23] (supplemental-Fig. 2). To reduce overfitting and improve generalizability, we grew a shallow tree by forcing the number of observations per leaf to be at least 10 or the number of splits per predictor to be at most 5. The number of ensembled trees ($=200$) was obtained from hyperparameter optimization. We implemented the proposed hierarchical feature selection algorithms on both linear and decision tree regression models. Additionally, the selected features from ElasticNet were fed to a multivariate generalized linear model and those selected based on PRFvI algorithm were tested in the decision-tree model. The model performance was evaluated based on nested CV tenfold R^2, mean-absolute-error (MAE), mean-relative-absolute-error (MRAE), and root-mean-square-error (RMSE) compared to ground truth.

We further tested sensitivity and specificity of the best model for predicting tumor absorbed dose >25 Gy/cycle for response. This threshold dose was chosen as it is a previously reported cutoff for adequate tumor response following ^{177}Lu-PRRT [24].

Results

A total of 25 patients (M14: F11, age 63.7 ± 9.5, range 38–76) with 90 neuroendocrine tumors larger than 2 mL (mean $= 65.6 \pm 139.9$ mL, range: 2.1–1039 mL) were included in this study. The majority of studied tumors were found in the liver (75/90), while 11 lesions were lymph node metastases. Three primary pancreas tumors and one chest tumor were also included. An example of corresponding ^{68}Ga-PET, post-treatment ^{177}Lu SPECT/CT, and resulting time-activity curves of target lesions are given in Fig. 1. PET-SUV_{mean} and SUV_{peak} measured from the 90 studied tumors were 16 ± 6.4 (5.6–34.2) and 26.4 ± 15.5 (6.1–104), respectively, while SUV_{mean} for normal liver, spleen and kidneys were 6.9 ± 2.4 (2.2–11.4), 13.1 ± 3.5 (7–19.2), and 5.4 ± 2.7 (5.4–19.2), respectively. The mean tumor absorbed dose averaged 2.68 ± 1.89 Gy/GBq (0.23–10.26 Gy/GBq), while the average value of T_{eff} was 91.6 ± 26.6 h (27.9–159.5 h). In order to reduce the absorbed dose calculation uncertainties owing to mis-registrations and partial

volume effects, we excluded lesions smaller than 4 mL (>4 mL, $N=80$) for the statistical analysis.

The total variable set, including 16 quantitative and 3 qualitative ^{68}Ga-PET features, 8 treatment history, and 11 blood-test biomarkers, is detailed in Table 1.

The statistical variability of the investigated predictors dichotomized based on ANOVA-test of the absorbed dose are illustrated in Table 2.

Self and cross-correlation of all baseline features compared to tumor absorbed dose and 4 other dose-related parameters (parameters that directly contribute to absorbed dose) is presented in Fig. 2 (Spearman-correlation (ρ), q-value <0.05). The dose-related parameters are the scale factor C of the time-activity curve normalized by tumor volume (C_{vol}), TIA normalized by tumor volume (TIA_{vol}) and T_{eff}. We expect a physics-informed correlation between absorbed dose and TIA_{vol}, according to the assumption of local-energy-deposition for ^{177}Lu-labeled agents [25], and hence a correlation with TIA_{vol} components (C_{vol} and T_{eff}). SUV_{mean} shows a strong correlation with dose parameters (dose: $\rho=0.64$, TIA: $\rho=0.39$, C_{vol}: $\rho=0.56$), followed by $TLSUV_{mean}$ (dose: $\rho=0.45$, TIA_{vol}: $\rho=0.51$, C_{vol}: $\rho=0.63$) and SUV_{peak} (dose: $\rho=0.41$, TIA_{vol}: $\rho=0.54$, C_{vol}: $\rho=0.56$). $TotLiverSUV_{mean}$ shows a correlation only with C_{vol} ($\rho=0.44$). A significant but moderate correlation between T_{eff} and the pre-PRRT number of systemic treatments (#Systemic therapy) ($\rho=-0.31$), capecitabine/temozolomide ($\rho=-0.35$) and bilirubin ($\rho=0.33$) is observed.

Figure 3 illustrates the intra-patient variability of the index tumor absorbed doses among the study population. The intra-patient tumor absorbed dose per unit administered activity variability in terms of coefficient of variation (CoV) was within the range of 0.04–0.78 (median $= 0.38$); this is comparable to the variation within the whole tumor-set, which had a CoV of 0.69.

Also, two lesions with unusually high uptakes (high absorbed dose lesions in P_22, P_25 in Fig. 3) were considered outliers and excluded from model building because of their exceptionally high uptake in 177Lu-SPECT, despite their ^{68}Ga-PET uptake in a similar range compared to the other analyzed lesions in the same patients.

The association of dose and different SUV parameters were evaluated using univariate analysis (linear least-square regression). SUV_{mean} (coefficient-of-determination: $R^2=0.28$), compared to SUV_{peak} ($R^2=0.07$), and SUV_TNRs ($R^2 \leq 0.12$) showed a better performance in prediction of delivered absorbed dose (Fig. 4). No significant differences of absorbed doses or SUV-parameters were observed based on tumor volume or localization.

We compared the prediction performance of multiple machine learning algorithms (linear and ensembled-tree) using PET-SUVs and biomarkers, summarized in Table 3. According to the proposed hierarchical feature-selection
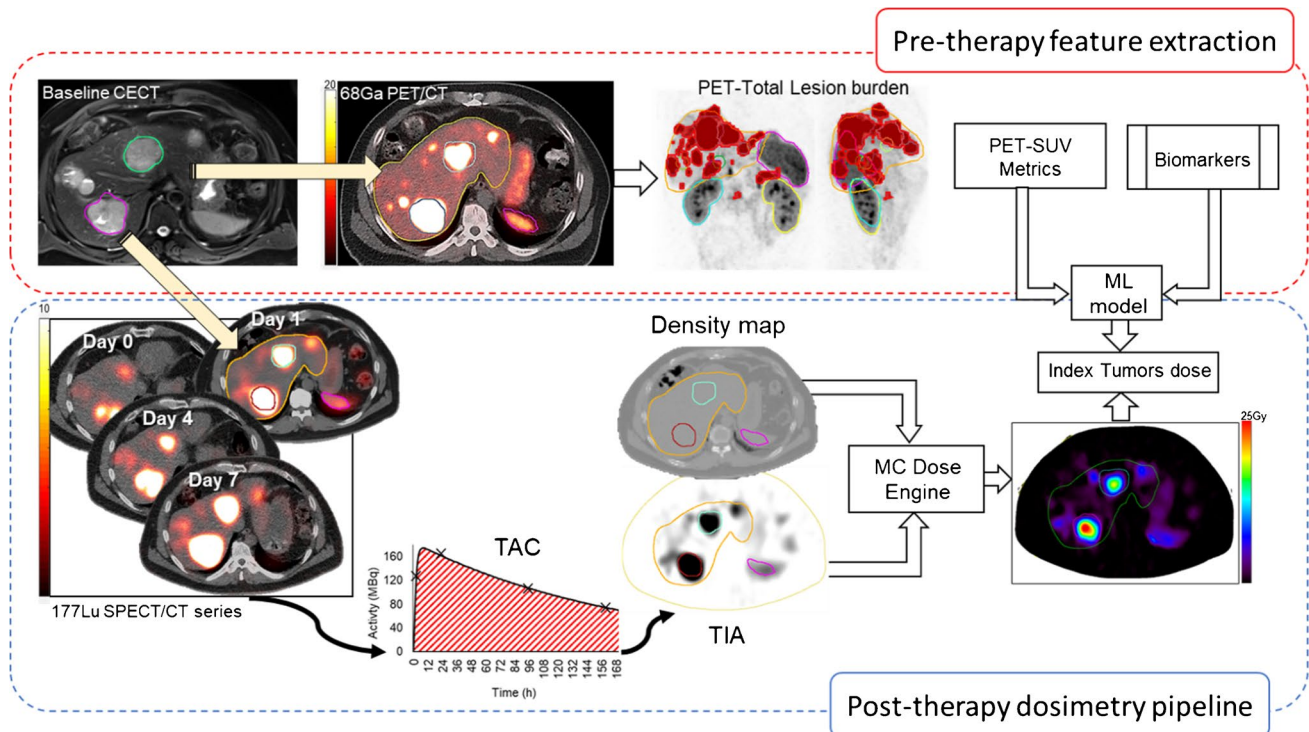
Fig. 1 Top panel: baseline diagnostic images (contrast-enhanced CT/MRI) were used to define target lesions, which were then co-registered to pretherapy ^{68}Ga-DOTATATE PET/CT and posttherapy 177Lu-DOTATATE SPECT/CT images. Bottom panel: dosimetry pipeline included four timepoints registration of SPECT images to generate TIA that is fed into MC-based dose engine

strategies (supplemental-Fig. 5), linear univariate regression model picked SUV_{mean} with $R^2 = 0.28$ and MAE = 1.08 Gy/GBq.

We compared a cross-combination of all features with SUV_{mean} to evaluate the second and third important features in dose prediction (supplemental-Figure 5 and 6). $TotLiverSUV_{mean}$ and $TLSUV_{mean}$ were the most effective predictors in terms of R^2 and MAE ($R^2 = 0.61$ and 0.48, MAE = 0.82 and 0.88 Gy/GBq, respectively) from Ensembled Tree (Ens-Tree) models. The best prediction performance was achieved from a trivariate Ens-Tree algorithm consisting of SUV_{mean}, $TotLiverSUV_{mean}$, and $TLSUV_{mean}$ with $R^2 = 0.64$ and MAE = 0.73 Gy/GBq (Table 3). The predicted absorbed dose compared with the measured absorbed dose from different algorithms is illustrated in Fig. 5.

The sensitivity and specificity of the best-performing model (trivariate Ens-Tree from Table 3 and Fig. 5), using a threshold of 25 Gy/cycle for response, was calculated as 0.82 and 0.94, respectively (Fig. 6). Again, this threshold-level was chosen to mirror previously reported dose-cutoffs for response following ^{177}Lu-PRRT [24]. A receiver operating characteristic (ROC) analysis was conducted to evaluate the performance of the proposed model with respect to the absorbed dose-cutoff. The area under the ROC curve (AUC) was 0.92.

Discussion

Accurate and early prediction of therapeutic absorbed dose in NETs is important information that can be used to guide appropriate patient selection and treatment alterations for PRRT, potentially helping to distinguish between patients likely to undergo effective versus futile treatments. To date, ^{68}Ga-PET derived quantitative metrics have appeared promising as a measure of SSTR2 density in neuroendocrine tumors [26]; however, studies assessing correlation between SUV features and absorbed dose/treatment outcomes remain scarce, and further investigation is necessary to establish conclusive relationships.

Prediction of tumor and organ-absorbed doses may help optimize treatment efficacy prior to therapy by enabling an individualized treatment plan, administering variable doses of PRRT that maximize tumor irradiation while minimizing organ exposure. According to a recent study indicating the decline of [^{177}Lu]Lu-DOTA-TATE tumor uptake over therapy cycles, an individualized dose escalation strategy may be more effective in the first cycle [10]. A clinical trial reported on personalized [^{177}Lu]Lu-DOTA-TATE PRRT guided by the prediction of renal toxicity based on eGFR and patient-surface-area prior to the therapy [5]. In our ongoing research with standard dose [^{177}Lu]Lu-DOTA-TATE, we have already

Table 2 Patients' clinicopathological biomarkers. The variability of the tumor absorbed dose per unit administered activity and SUV_mean with respect to the dichotomized predictors is illustrated. The forest-plot represents the range of dose values in the selected predictor's group while dots represent mean dose values. *P* value was obtained from ANOVA test. The dichotomization cutoffs of the continuous predictors were calculated from an iterative process (1000 iterations), in which a random number within the range of predictor's quantiles (0.05–0.95) were generated to binarize the predictor values. Then, one-way ANOVA test was applied on dose vector according to the binarized predictor; thus, the cutoff was selected based on the minimum *p* value obtained from ANOVA-test

| Parameters	N (%)	Mean ± std	SUVmean	Dose (Gy/GBq)	P_val
Volume					
≤52 mL	70	15.07 ± 10.6	20.74 ± 8.6		0.13
>52 mL	30	177.07 ± 217.5	17.93 ± 6.7		
SUV_CoV					
≤ 45 %	68	0.30 ± 0.1	19.51 ± 7.9		0.02
> 45 %	32	0.55 ± 0.1	20.70 ± 8.7		
TLV (mL)					
≤ 150	10	60.87 ± 42.6	23.30 ± 8.6		<0.001
> 150	90	624.30 ± 664.4	19.52 ± 8.0		
TL-SSE (SUV.mL)					
≤ 2864	30	1683 ± 763	16.30 ± 7.5		0.001
> 2864	70	12005 ± 9895	21.44 ± 7.9		
White blood cells					
≤ 5.4	35	3.57 ± 0.8	21.26 ± 10.1		0.08
> 5.4	65	8.16 ± 2.1	19.16 ± 6.8		
Lymphocytes					
≤ 1.6	64	0.91 ± 0.4	19.73 ± 8.5		0.04
> 1.6	36	1.95 ± 0.3	20.19 ± 7.5		
Absolute neutrophil					
≤ 2	18	1.62 ± 0.2	21.91 ± 9.8		0.03
> 2	82	4.54 ± 1.5	19.47 ± 7.7		
Hemoglobin					
≤ 12	20	11.24 ± 0.9	18.71 ± 10.1		0.01
> 12	80	13.70 ± 1.0	20.20 ± 7.6		
Platelet					
≤ 190	29	167.81 ± 19.3	19.40 ± 9.4		0.008
> 190	71	255.90 ± 59.4	20.10 ± 7.6		
eGFR					
≤ 52	12	40.26 ± 10.6	16.47 ± 7.3		0.04
> 52	88	82.46 ± 14.0	20.39 ± 8.2		
Creatinine					
≤ 1.2	81	0.89 ± 0.2	20.67 ± 8.1		0.03
> 1.2	19	1.39 ± 0.3	16.56 ± 7.5		
Bilirubin					
≤ 0.9	81	0.49 ± 0.2	20.18 ± 8.0		0.08
> 0.9	19	1.13 ± 0.1	18.67 ± 8.9		
Albumin					
≤ 4.5	68	4.04 ± 0.3	20.86 ± 7.8		<0.001
> 4.5	32	4.88 ± 0.3	17.91 ± 8.5		
Alkaline phosphatase					
≤ 88	20	74.57 ± 13.7	23.21 ± 8.2		
> 88	80	149.91 ± 40.3	19.07 ± 7.9		<0.001
CgA					
≤ 500	28	146.60 ± 140.6	25.91 ± 8.1		0.001
> 500	72	3434.12 ± 7070.4	17.62 ± 6.9		
Grade					
G=1	33		22.16 ± 9.8		0.3
G ≥ 2	67		18.69 ± 7.0		
Bone Met					
No	51		20.85 ± 7.5		0.12
Yes	49		18.90 ± 8.7		
Nodal Met					
No	29		23.22 ± 8.5		0.14
Yes	71		18.56 ± 7.6		
# Systemic therapy					
0	52		17.90 ± 5.5		0.54
1 or 2	42		20.99 ± 9.2		
≥ 2	5		31.56 ± 11.3		
Primary tumor site					
Midgut	61		19.40 ± 7.8		0.79
Pancreas	28		22.84 ± 9.2		
Other	11		15.43 ± 4.0		

Dose (Gy/GBq) axis: 0   2   4   6
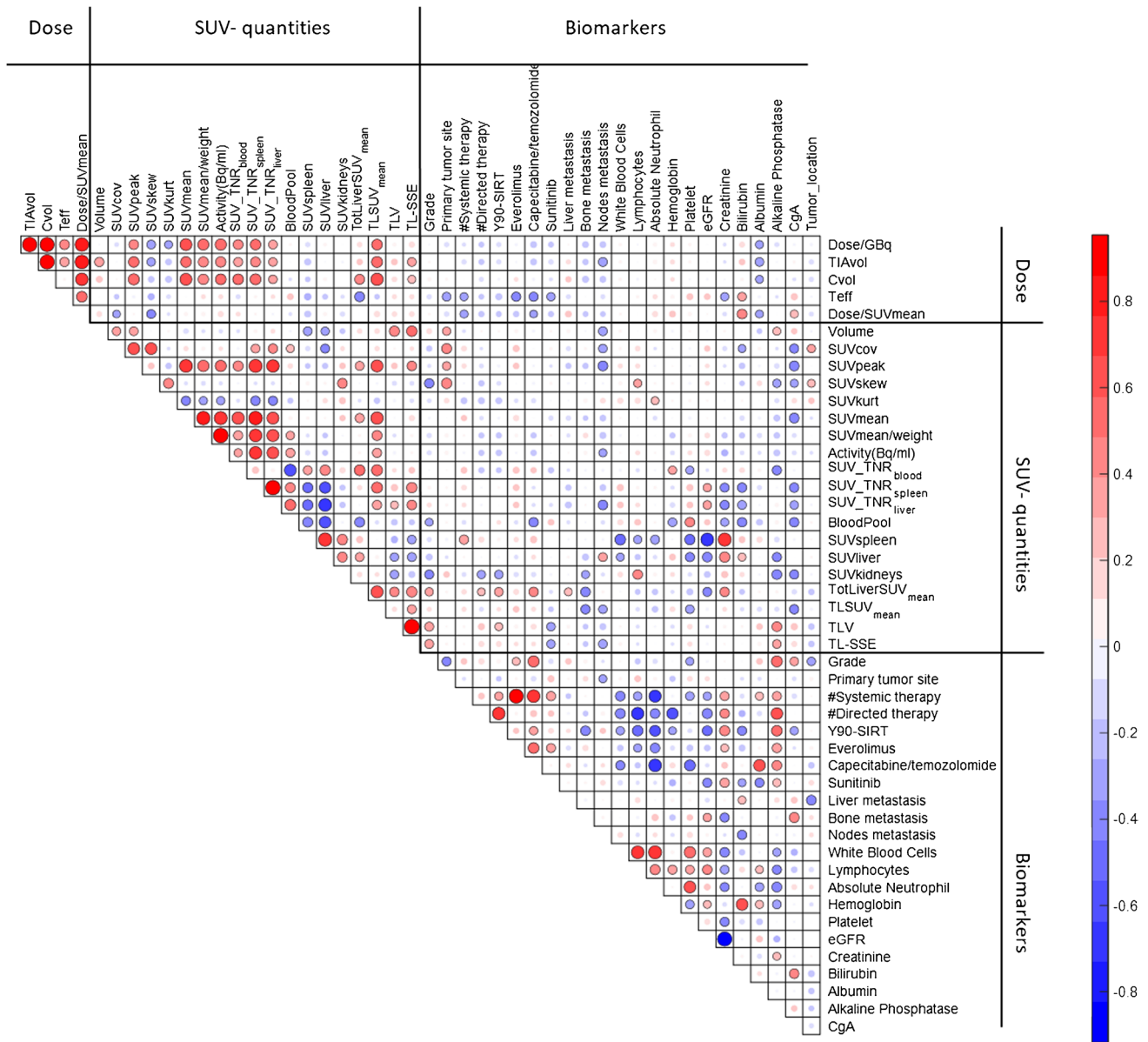
Fig. 2 Spearman rank self and cross correlation between absorbed dose-related parameters (dose, TIA_{vol}, C_{vol} and T_{eff}) and PET-SUV parameters along with biomarkers. The color code and size of spheres show the correlation magnitude. The insignificant correlations (q-value > 0.05) are plotted as faded spheres

developed a predictive model for kidney absorbed dose based on pretherapy PET-SUV metrics and biomarkers (i.e., eGFR) estimating posttherapy renal absorbed dose within 18% accuracy [9]. In the current study, we further evaluated the predictive power of ^{68}Ga-PET SUV metrics with readily available baseline biomarkers to develop machine learning models for tumor absorbed dose prediction.

The relationship between baseline PET-derived features and delivered absorbed dose is not straightforward. First, there are notable differences in the pharmacokinetics and biodistribution of ^{68}Ga/^{177}Lu-DOTATATE theragnostic pairs [2], influenced by variable masses and

chemical structures of administered radiopharmaceuticals, patient behavior [4], radioactive metabolites [27], medication effects, etc. Second, the static ^{68}Ga-PET acquisition (~ 60 min post-injection) potentially only depicts the SSTR2 density distribution, while the absorbed dose quantity is related to dynamic physiologic circulation and accumulation of the radiopharmaceutical. In the other word, dose quantity is proportional to the multiplication of C_{vol} (scale factor of the time-activity curve normalized by tumor volume) and T_{eff} (retention half-life).

In this context, we observed a significant correlation of PET-SUV metrics with C_{vol} (Figs. 2, 3, SUV_{mean}: $\rho = 0.63$),
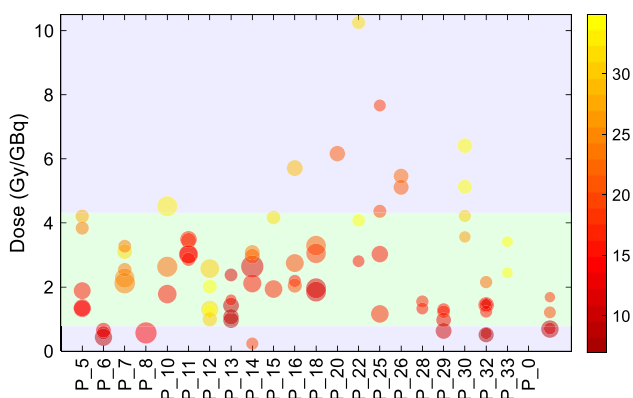
Fig. 3 Intra-patient variability of tumor absorbed doses per unit administered activity for all patients. The sphere color indicates SUV_{mean}, and background color shows the margins of standard deviation of tumor absorbed dose per unit administered activity values. The size of spheres depicts the volume of tumors in logarithmic form (4–1039 mL)

There is a body of literature that indicated a significant correlation between ^{68}Ga-SUV and ^{177}Lu-induced tumor absorbed dose [7, 15, 28]. Ezziddin et al. reported a strong correlation between ^{68}Ga-DOTATOC SUV-metrics with [^{177}Lu]Lu-Octreotate absorbed dose (SUVmean: $\rho = 0.72$; SUVmax: $\rho = 0.71$) [28]. Hänscheid et al. showed that PET-based SUVmax significantly correlates ($\rho = 0.76$) with the maximum absorbed dose delivered to tumor in meningioma patients [29]. However, one group, Singh et al. found no significant correlation between SUVs and the tumor absorbed dose from [^{177}Lu]Lu-DOTA-TATE therapy in metastatic-NETs [26].

In previous studies, tumor-to-normal organ ratios (SUV_TNRs) were suggested as potential factors that might reduce the inter-patient and inter-acquisition variability associated with tumor SUV by using physiological uptake in normal organs as an individualized reference [30–32]. We compared the correlation of tumor SUV, SUV_TNRs, and activity concentration with respect to absorbed dose, but SUV_{mean} outperformed other metrics in terms of strength of the correlation (Fig. 4 and supplemental-Fig. 4). We have previously noted discordance using TNR between the ^{68}Ga PET and the 177-Lu-PRRT dosimetry SPECT/CT, with significantly higher SUV TNR on ^{177}Lu SPECT compared with ^{68}Ga PET [2]. This phenomenon may be related to temporal differences

while no correlation with T_{eff} (Supplemental-Fig. 3-4). Therefore, it can be concluded that the observed correlation between PET-SUV parameters and the tumor absorbed dose quantity (SUV_{mean}: $\rho = 0.62$) stems from the correlation between ^{68}Ga-tumor-uptake and ^{177}Lu-tumor-uptake.
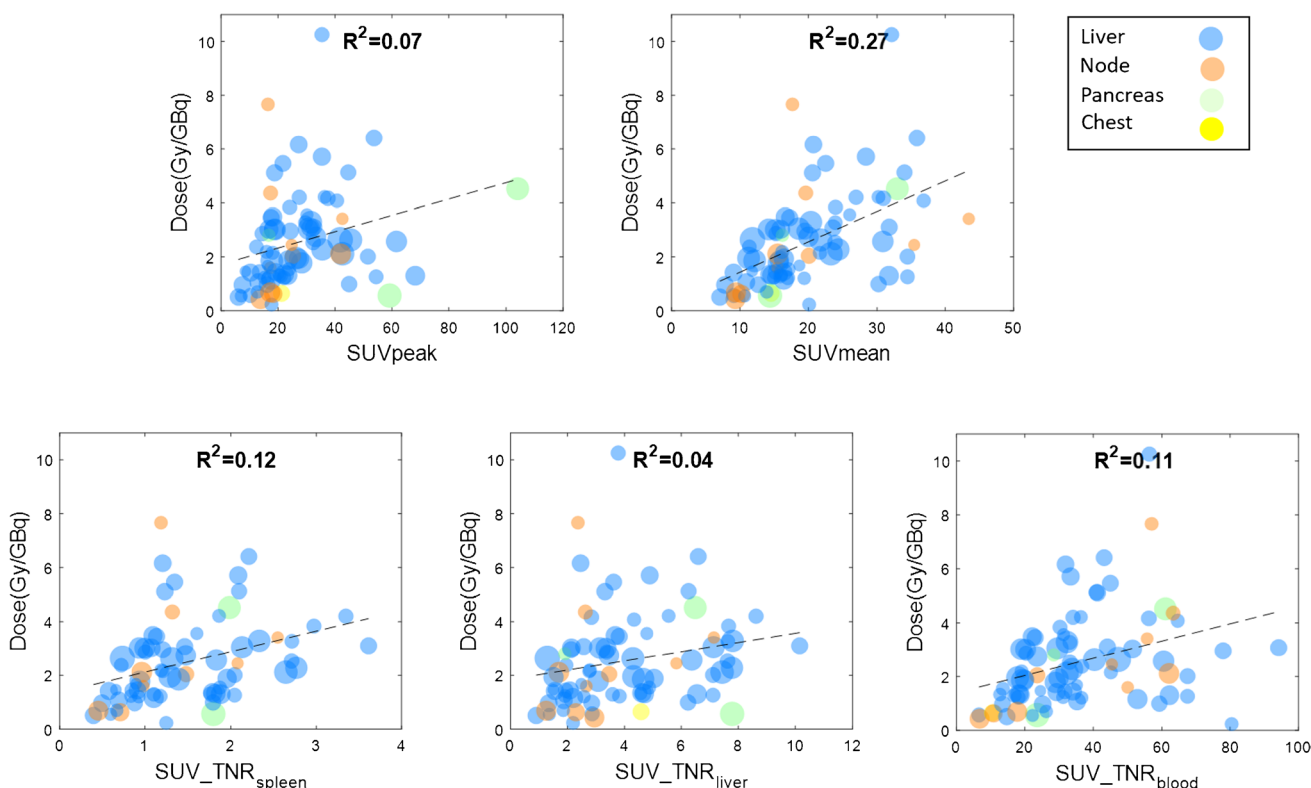

Fig. 4 Tumor absorbed dose plotted vs. tumor PET-SUV quantities, where the color shows the tumor location. The size of spheres depicts the volume of tumors in logarithmic form (4–1039 mL)

Table 3 Model performance of the selected prediction algorithms using ^{68}Ga-PET SUV metrics. The quantitative metrics are reported as mean (95% CI) calculated from nested CV. The MAE quantile range is reported based on the averaging over 10-outerloop CV point prediction

Model	Features	R^{2*} tenfold	Median MRAE	MAE (Gy/GBq)	MAE quantile (0.05–0.95)	RMSE (Gy/GBq)
Univariate	Linear					
	SUV_{mean}	0.28(0.00)	0.38(0.00)	1.08(0.00)	0.14–2.8	1.44
Bivariate	Tree_Ens					
	SUV_{mean}, $TotLiverSUV_{mean}$	0.61(0.01)	0.26(0.01)	0.82(0.01)	0.10–2.29	1.33
	SUV_{mean}, $TLSUV_{mean}$	0.48(0.03)	0.26(0.01)	0.88(0.02)	0.05–2.66	1.35
Trivariate	Tree_Ens					
	SUV_{mean}, $TotLiverSUV_{mean}$, $TLSUV_{mean}$	0.64(0.02)	0.20(0.01)	0.73(0.02)	0.02–2.46	1.28

*Two outliers are excluded from reported R^2

in DOTATATE uptake and internalization in tumor as compared to normal organs, further accentuated by differences in image timing (60 min PET vs. > 4 h SPECT/CT) [2].

We evaluated the correlation of inter-patient PET-derived total lesion burden metrics, including total lesion volume (TLV), average SUV of the total lesion volume ($TLSUV_{mean}$), and total lesion somatostatin expression (TL-SSE = TLV × TL-SUV_{mean}), all compared to the index tumor absorbed dose (Fig. 2). $TLSUV_{mean}$ showed a strong correlation with dose components (C_{vol}: $\rho > 0.63$), while no significant correlation

was observed regarding TLV and TL-SSE. This association is reasonable from a physiologic standpoint, given that greater overall PET tracer avidity may correlate to increased PRRT binding and dose deposition by a similar theragnostic pair. Accordingly, a recent paper notably found correlation of $TLSUV_{mean}$ with survival in NET patients treated by [^{177}Lu]Lu-DOTATATE, implicitly showing correlation of $TLSUV_{mean}$ with tumor absorbed dose and accordingly therapy-response [33]. Furthermore, we found a strong correlation between SUV_{mean} of the total liver volume ($TotLiverSUV_{mean}$) with dose

Fig. 5 Pretherapy predicted absorbed dose using univariate linear model and random forest (RF) bi/tri-variate models of Table 2 vs. the delivered dose measured from Lu-177 SPECT/CT (the filled gray dots represent the 2 outliers)
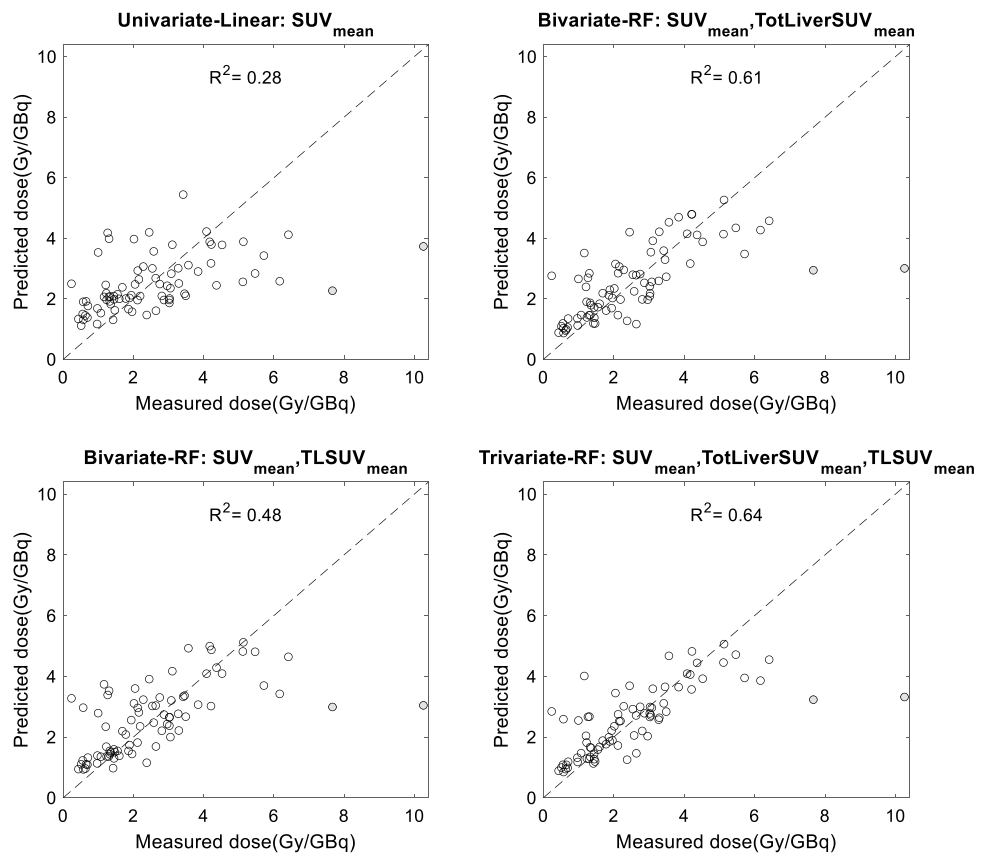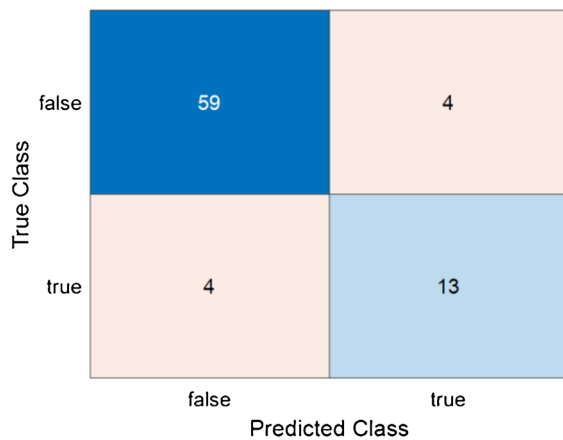
Fig. 6 Considering the threshold absorbed dose for responders of 25 Gy/cycle, confusion matrix of predicted absorbed dose from trivariate Ens-Tree model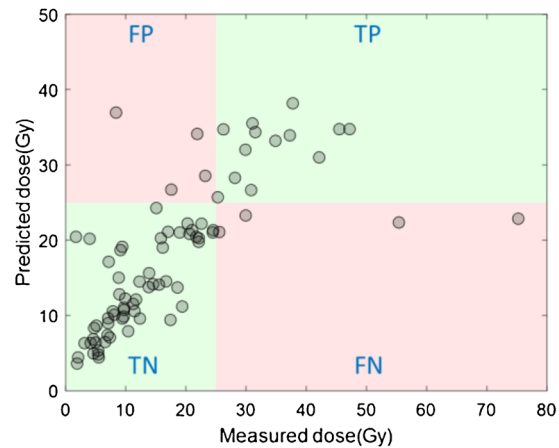 compared to the measured absorbed dose (left). Sensitivity ($\frac{TP}{TP+FN}$) and specificity ($\frac{TN}{FP+TN}$) visualization of the predcition model (right). TP true-positive, FP false-positive, TN true-negative, FN false-negative

components (C_{vol}: $\rho = 0.45$). We used $TotLiverSUV_{mean}$ as a surrogate for extent of hepatic metastatic disease involvement.

$$TotLiverSUV_{mean} = \frac{(tumor\_liver\_SUV_{mean} \times Tumor\_volume) + (healthy_{liverSUV_{mean}} \times healthy\_liver\_volume)}{(healthy + tumor)\ liver\ volume}.$$

By expanding a univariate analysis showing the predictive value of SUV_{mean}, we built bi/tri-variate models to enhance prediction accuracy. The best model performance achieved by a trivariate model composed of only PET-SUV metrics: SUV_{mean}, $TotLiverSUV_{mean}$, and $TLSUV_{mean}$. All three metrics showed strong correlation with radiopharmaceutical-uptake-related dose component (C_{vol}), illustrated in supplemental-Fig. 7. A bivariate model only using SUV_{mean} and $TotLiverSUV_{mean}$ likewise showed a good predictive performance ($R^2 = 0.61$, MAE = 0.82 Gy/GBq). These results illustrate that the extent of liver tumor involvement, via $TotLiverSUV_{mean}$, is predictive of absorbed dose. The main advantage of using this variable is that it is readily calculated from PET images without any complicated computation: it is merely the SUV_{mean} of entire liver segmented volume, which can be simply performed through machine learning models from CT images. According to Figs. 5 and 6, about 17% of tumors with low absorbed doses (~ 7 ± 4.8 Gy) are overestimated; while, about 2.5% of tumors with very high absorbed doses (> 55 Gy) are underestimated (|MRAE| > 0.5).

In addition to Ens_Tree models, we evaluated bi- and tri-variate linear models, where SUV_{mean} combined with bilirubin and albumin improved the prediction performance ($R^2 = 0.47$, MAE = 0.87 Gy/GBq). Bilirubin and prior systemic treatment showed significant correlations with T_{eff} ($\rho = -0.33$ and $\rho = 0.3$, respectively). These findings may suggest that prior treatments or underlying hepatic dysfunction may alter tumor behavior and potentially the degree of PRRT tumor uptake and metabolism. Despite the observed

correlation between prior-systemic-treatment and bilirubin with respect to T_{eff}, (Fig. 2 and Supplemental-Fig. 4) the indirect impact of these two biomarkers on tumor absorbed dose that is composed of two components (i.e., C_{vol} and T_{eff}) was not significant. Our linear model, built upon the features selected by ElasticNet (7 variables), also showed some improvement compared to trivariate linear models ($R^2 = 0.57$, MAE = 0.8 Gy/GBq), but due to a higher number of model-variables, it is prone to spurious correlations in a small-size dataset. The features selected by PRFvI algorithm align with those from the hierarchical algorithm; however, compared to trivariate decision tree, the model performance did not show any improvement (supplemental-Fig. 8).

Tumor absorbed dose in PRRT is likely influenced by multiple biological factors, both individual patient characteristics and specific tumor features (i.e., proliferation rate, heterogeneity, intrinsic radio-sensitivity). The intra-patient tumor absorbed dose per unit administered activity variability of our dataset is comparable with inter-patient variability of the whole set (0.38 vs. 0.69); therefore, we treated each individual tumor independently, while the biomarkers and some PET features, such as TL-SSE and $TLSUV_{mean}$ were calculated in the patient-level, feeding inter-patient information to our models.

The primary limitations of our study are its small sample size and lack of independent multi-center validation and back-testing of the models, relying instead on nested cross validation. Although we followed the recommended rules for generalizability and interpretability of the models [21], further investigation is warranted. Interpretations of dose metrics involving ^{177}Lu-PRRT are challenging due to the lack of complete understanding between the dose quantities and clinical end points. Currently, dose-response models are extrapolated from external beam radiotherapy (e.g., kidney

dose-limit of 23 Gy or 28 Gy [34, 35]) or other RPTs, both with non-negligible radiobiologic differences. An inherent limitation of these studies relates to the uncertainties associated with quantitative imaging (i.e., scatter/attenuation correction, segmentation, and partial volume correction) and multi-timepoint serial imaging to determine kinetics (i.e., time-series registration) [17]. In addition, simplification in posttherapy imaging such as using SPECT-planar hybrid imaging or reduced timepoints or approximation in particle transport algorithms can introduce extra uncertainties into dosimetry process [36]. To the best of our knowledge, this is the first study of predictive dosimetry using complete four-timepoint posttherapy 3D SPECT/CT imaging, radiologist-defined lesion contours, and a validated Monte Carlo-based dosimetry workflow that reduces some of these uncertainties in the measured absorbed dose and hence help to build a more precise model. As post-PRRT imaging is increasingly used as part of routine clinical protocols at some centers, we expect more data to be available in the future to independently validate and improve the proposed model.

Conclusion

We investigated the predictive value of using ^{68}Ga-PET-based SUV metrics along with biomarkers to estimate the tumor absorbed dose with [^{177}Lu]Lu-DOTA-TATE therapy. We showed that tumor SUV_{mean}, $TotLiverSUV_{mean}$, and average SUV of the total lesion volume ($TLSUV_{mean}$) are capable of predicting the ^{177}Lu-PRRT delivered tumor absorbed dose with an accuracy of MAE = 0.71 Gy/GBq ($R^2 = 0.64$) in nested cross validation. We hope to further test the proposed models on multi-center data, to eventually provide a validated decision-support tool for clinicians to improve patient-selection and thus optimize treatment outcomes. Developing such precise quantitative metrics establishes a greater role of ^{68}Ga-PET for patient stratification, as well as prognostication and assessment of the therapeutic response modeling.

Declarations

Informed consent Informed consent was obtained from all individual participants included in the study.

Conflict of interest The authors declare no competing interests.

References

1. Baum RP, Kulkarni HR. Theranostics: from molecular imaging using Ga-68 labeled tracers and PET/CT to personalized radionuclide therapy - the Bad Berka experience. Theranostics. 2012;2(5):437–47.
2. Wong KK, et al. Differences in tumor-to-normal organ SUV ratios measured with 68Ga-DOTATATE PET compared with 177Lu-DOTATATE SPECT in patients with neuroendocrine tumors. Nucl Med Commun. 2022;43(8):892–900.
3. Strosberg J, et al. Phase 3 Trial of (177)Lu-dotatate for midgut neuroendocrine tumors. N Engl J Med. 2017;376(2):125–35.
4. Miller C, et al. Implications of physics, chemistry and biology for dosimetry calculations using theranostic pairs. Theranostics. 2022;12(1):232–59.
5. Del Prete M, et al. Personalized (177)Lu-octreotate peptide receptor radionuclide therapy of neuroendocrine tumours: initial results from the P-PRRT trial. Eur J Nucl Med Mol Imaging. 2019;46(3):728–42.
6. Sundlöv A, et al. Phase II trial demonstrates the efficacy and safety of individualized, dosimetry-based (177)Lu-DOTATATE treatment of NET patients. Eur J Nucl Med Mol Imaging. 2022;49(11):3830–40.
7. Xue S, et al. Application of machine learning to pretherapeutically estimate dosimetry in men with advanced prostate cancer treated with (177)Lu-PSMA I&T therapy. Eur J Nucl Med Mol Imaging. 2022;49(12):4064–72.
8. Peters SMB, et al. [(68)Ga]Ga-PSMA-11 PET imaging as a predictor for absorbed doses in organs at risk and small lesions in [(177)Lu]Lu-PSMA-617 treatment. Eur J Nucl Med Mol Imaging. 2022;49(4):1101–12.
9. Peterson AB, et al. 177Lu-DOTATATE Theranostics: predicting renal dosimetry from pretherapy 68Ga-DOTATATE PET and clinical biomarkers. Clin Nucl Med. 2023;48(5):393–9.
10. Roth D, et al. Dosimetric quantities in neuroendocrine tumors over treatment cycles with (177)Lu-DOTATATE. J Nucl Med. 2022;63(3):399–405.
11. Lassmann M, Eberlein U. The relevance of dosimetry in precision medicine. J Nucl Med. 2018;59(10):1494–9.
12. Ilan E, et al. Dose response of pancreatic neuroendocrine tumors treated with peptide receptor radionuclide therapy using 177Lu-DOTATATE. J Nucl Med. 2015;56(2):177–82.
13. Öksüz M, et al. Peptide receptor radionuclide therapy of neuroendocrine tumors with (90)Y-DOTATOC: is treatment response predictable by pre-therapeutic uptake of (68)Ga-DOTATOC? Diagn Interv Imaging. 2014;95(3):289–300.
14. Ambrosini V, et al. Prognostic Value of 68Ga-DOTANOC PET/CT SUVmax in patients with neuroendocrine tumors of the pancreas. J Nucl Med. 2015;56(12):1843–8.
15. Bruvoll R, et al. Correlations between [(68)Ga]Ga-DOTA-TOC uptake and absorbed dose from [(177)Lu]Lu-DOTA-TATE. Cancers (Basel) 2023;15(4).
16. Stenvall A, et al. Relationships between uptake of [(68)Ga]Ga-DOTA-TATE and absorbed dose in [(177)Lu]Lu-DOTA-TATE therapy. EJNMMI Res. 2022;12(1):75.
17. Dewaraja YK, et al. A pipeline for automated voxel dosimetry: application in patients with multi-SPECT/CT imaging after (177)Lu-peptide receptor radionuclide therapy. J Nucl Med. 2022;63(11):1665–72.
18. Tran-Gia J, Lassmann M. Characterization of noise and resolution for quantitative (177)Lu SPECT/CT with xSPECT Quant. J Nucl Med. 2019;60(1):50–9.

19. Wilderman SJ, Dewaraja YK. Method for fast CT/SPECT-Based 3D Monte Carlo absorbed dose computations in internal emitter therapy. IEEE Trans Nucl Sci. 2007;54(1):146–51.

20. Cui S, et al. Combining handcrafted features with latent variables in machine learning for prediction of radiation-induced lung damage. Med Phys. 2019;46(5):2497–511.

21. Peduzzi P, et al. Importance of events per independent variable in proportional hazards regression analysis. II. Accuracy and precision of regression estimates. J Clin Epidemiol. 1995;48(12):1503–10.

22. Breiman L. Random forests. Mach Learn. 2001;45(1):5–32.

23. Lou Y, Caruana R, Gehrke J. Intelligible models for classification and regression. In: Proceedings of the 18th ACM SIGKDD international conference on knowledge discovery and data mining. Beijing: Association for Computing Machinery; 2012. p. 150–158

24. Del Prete M, Buteau FA, Beauregard JM. Personalized (177)Lu-octreotate peptide receptor radionuclide therapy of neuroendocrine tumours: a simulation study. Eur J Nucl Med Mol Imaging. 2017;44(9):1490–500.

25. Sjögreen Gleisner K, et al. EANM dosimetry committee recommendations for dosimetry of 177Lu-labelled somatostatin-receptor- and PSMA-targeting ligands. Eur J Nucl Med Mol Imaging. 2022;49(6):1778–809.

26. Singh B, et al. Can the standardized uptake values derived from diagnostic 68 Ga-DOTATATE PET/CT imaging predict the radiation dose delivered to the metastatic liver NET lesions on 177 Lu-DOTATATE peptide receptor radionuclide therapy? J Postgrad Med Edu Res. 2013;47:7–13.

27. Lubberink M, et al. In vivo instability of (177)Lu-DOTATATE during peptide receptor radionuclide therapy. J Nucl Med. 2020;61(9):1337–40.

28. Ezziddin S, et al. Does the pretherapeutic tumor SUV in 68Ga DOTATOC PET predict the absorbed dose of 177Lu octreotate? Clin Nucl Med. 2012;37(6):e141–7.

29. Hänscheid H, et al. PET SUV correlates with radionuclide uptake in peptide receptor therapy in meningioma. Eur J Nucl Med Mol Imaging. 2012;39(8):1284–8.

30. Ilan E, et al. Tumor-to-blood ratio for assessment of somatostatin receptor density in neuroendocrine tumors using (68)Ga-DOTATOC and (68)Ga-DOTATATE. J Nucl Med. 2020;61(2):217–21.

31. Kroiss A, et al. 68Ga-DOTA-TOC uptake in neuroendocrine tumour and healthy tissue: differentiation of physiological uptake and pathological processes in PET/CT. Eur J Nucl Med Mol Imaging. 2013;40(4):514–23.

32. Kim YI, et al. Tumour-to-liver ratio determined by [(68)Ga]Ga-DOTA-TOC PET/CT as a prognostic factor of lanreotide efficacy for patients with well-differentiated gastroenteropancreatic-neuroendocrine tumours. EJNMMI Res. 2020;10(1):63.

33. Pauwels E, et al. [(68)Ga]Ga-DOTATATE-avid tumor volume, uptake and inflammation-based index correlate with survival in neuroendocrine tumor patients treated with [(177)Lu]Lu-DOTATATE PRRT. Am J Nucl Med Mol Imaging. 2022;12(5):152–62.

34. Emami B, et al. Tolerance of normal tissue to therapeutic irradiation. Int J Radiat Oncol Biol Phys. 1991;21(1):109–22.

35. Dawson LA, et al. Radiation-associated kidney injury. Int J Radiat Oncol Biol Phys. 2010;76(3 Suppl):S108–15.

36. Akhavanallaf A, et al. Whole-body voxel-based internal dosimetry using deep learning. Eur J Nucl Med Mol Imaging. 2021;48(3):670–82.

Authors and Affiliations

Azadeh Akhavanallaf[1,2] · **Avery B. Peterson**[1] · **Kellen Fitzpatrick**[1] · **Molly Roseland**[1] · **Ka Kit Wong**[1] · **Issam El-Naqa**[3] · **Habib Zaidi**[2,4,5,6] · **Yuni K. Dewaraja**[1]

[1] Department of Radiology, University of Michigan, 1301 Catherine, 2276 Medical Science I/5610, Ann Arbor, MI 48109, USA

[2] Division of Nuclear Medicine and Molecular Imaging, Geneva University Hospital, CH-1211 Geneva, Switzerland

[3] Department of Machine Learning, Moffitt Cancer Center, Tampa, FL, USA

[4] Geneva University Neurocenter, Geneva University, CH-1205 Geneva, Switzerland

[5] Department of Nuclear Medicine and Molecular Imaging, University Medical Center Groningen, University of Groningen, 9700 RB Groningen, Netherlands

[6] Department of Nuclear Medicine, University of Southern Denmark, DK-500 Odense, Denmark